Journal of Power Sources 189 (2009) 51–58

Contents lists available at ScienceDirect

Journal of Power Sources

journal homepage: www.elsevier.com/locate/jpowsour

In-situ XAS study on Li_2MnSiO_4 and Li_2FeSiO_4 cathode materials

R. Dominko[a,*], I. Arčon[b,c], A. Kodre[c,d], D. Hanžel[c], M. Gaberšček[a,e]

[a] National Institute of Chemistry, Hajdrihova 19, SI-1000 Ljubljana, Slovenia
[b] University of Nova Gorica, Vipavska 13, P.O. Box 301, SI-5001, Nova Gorica, Slovenia
[c] Jozef Stefan Institute, Jamova 39, SI-1000 Ljubljana, Slovenia
[d] Faculty of Mathematics and Physics, Jadranska 19, SI-1000 Ljubljana, Slovenia
[e] Faculty of Chemistry and Chemical Technology, Aškerčeva 5, SI-1000 Ljubljana, Slovenia

ARTICLE INFO

Article history:
Received 24 June 2008
Received in revised form 8 September 2008
Accepted 20 November 2008
Available online 28 November 2008

Keywords:
Li_2FeSiO_4
Li_2MnSiO_4
In-situ Mössbauer spectroscopy
In-situ EXAFS
In-situ XANES
Li-ion batteries

ABSTRACT

Li_2FeSiO_4/C and Li_2MnSiO_4/C cathode materials were a subject of in-situ characterisations during the first cycle of oxidation/reduction by complementary techniques of X-ray absorption spectroscopy and Mössbauer spectroscopy, whereby the changes in the local environment of Fe (and Mn) are monitored. Both techniques demonstrate the reversibility of monitored parameters of Fe environment during lithium exchange, and hence confirm the cycling stability of the Li_2FeSiO_4/C. The position of Fe in slightly distorted oxygen tetrahedra shifts with the change of valence accompanying Li removal. Outside of the immediate oxygen envelope, in more distant coordination shells, only minor variation in the neighbour distances is detected, apparently due to a slight relaxation of the structure. The oxidation state of Mn in Li_2MnSiO_4/C cathode material changes from the initial Mn(II) to Mn(III) in the potential range from 4.0 to 4.5 V vs. lithium reference but not beyond. During the oxidation, the short Mn—O bond decreases from 2.04 to 1.87 Å in the correlation with the increase of Mn valence state, while the larger Mn—O distance in the MnO_4 tetrahedron remains unchanged. The reduction is not completely reversible as evident from the distribution of O atoms in the MnO_4 tetrahedron after one oxidation/reduction cycle.

1. Introduction

Some members of the family of Li-orthosilicates Li_2MSiO_4 (M = Mn, Fe, Co) together with their solid solutions have been recently prepared for structural and electrochemical characterisation for the potential use in Li-ion batteries [1–4]. This type of cathode material is attractive in view of a possible exploration of both lithium equivalents from the structure which would in practice lead to capacities with theoretical limit at 330 mA h g^{-1}. Furthermore, the thermally stable orthosilicate cathode materials, built of abundant elements Si, Fe and Mn, provide cheap cathode materials for large scale batteries that can operate at higher temperatures [5].

Orthosilicates can be considered as members of polyanion-type cathode materials [6]. The first report on Li_2FeSiO_4 by Nyten was followed by explanation of the mechanism of lithium exchange during the first two cycles [7] and of stability behaviour of Fe based orthosilicates [8]. Independently we have reported on structural and electrochemical characterisations of Li_2MnSiO_4 and Li_2FeSiO_4 [2,9–11]. Recently electrochemical characterisations of $Li_2(Mn,Fe)SiO_4$ solid solution and Li_2CoSiO_4 materials have been published [3,4].

Li_2MSiO_4 (M = Mn, Fe, Co) materials are iso-structural to lithium phosphate (Li_3PO_4) and can crystallize at least in eight polymorphs [3]. As-prepared samples are usually mixtures of polymorphs due to small difference in formation energy. Some polymorphs, however, can be isolated with selective synthesis conditions [12]. Although Li_2FeSiO_4 and Li_2MnSiO_4 are iso-structural, their electrochemical activities are different [13]. Lithium extraction/insertion process in Li_2FeSiO_4 is completely reversible with a lowering of the potential plateau from 3.10 to 2.80 V during the first cycle. This phenomenon was studied by in-situ XRD and in-situ Mössbauer spectroscopy, often used for study of Fe-based materials [14,15]. From these in-situ techniques a possible mechanism of the voltage shift in the oxidation process during lithium removal from Li_2FeSiO_4 has been proposed [7]. A more detailed in-situ XRD study has confirmed the reversible two-phase mechanism [14]. Lithium extraction (oxidation process) from Li_2MnSiO_4 occurs at the potential close to 4.1 V vs. metallic lithium [16]. It is followed by a change in the shape of the electrochemical curve during subsequent reduction/oxidation cycles, accompanied by an irreversible loss [9,10]. In-situ XRD experiment shows loss of intensities of Bragg reflections during first oxidation which are not retained after consequent reduction. More detailed studies on the local environment can be performed by in-

* Corresponding author. Tel.: +386 14760362; fax: +386 14760422.
E-mail address: Robert.Dominko@ki.si (R. Dominko).

0378-7753/$ – see front matter © 2008 Elsevier B.V. All rights reserved.
doi:10.1016/j.jpowsour.2008.11.077

situ X-ray absorption spectroscopy (XAS), namely XAS as a tool to investigate a local environment and electronic properties of electrode materials is becoming important characterization technique [17,18].

To elucidate the possible mechanism(s) during lithium extraction/insertion in Li_2FeSiO_4 and Li_2MnSiO_4 we performed in-situ XAS studies of the local environment and oxidation state of Fe and Mn cations upon lithium exchange, complemented by Mössbauer spectroscopic studies of Li_2FeSiO_4. All measurements were performed with the aim to understand the difference in the electrochemical behaviour.

2. Experimental

Li_2MnSiO_4/C and Li_2FeSiO_4/C were synthesised by standard Pechini synthesis [19]. The samples preparation has been recently described elsewhere [14]. Electrodes for in-situ XAS and in-situ Mössbauer spectroscopy were prepared by ball-milling the active material with 10 wt.% of acetylene black and 10 wt.% of EPDM in *n*-hexane. The obtained slurry was dried on 16 mm Al discs and the typical mass of active material was 30 mg. Prior the use, the electrodes were left at 90 °C in vacuum during the night. The in-situ cell consisted of two electrodes vacuum-sealed in triplex foil (coffee bag foil). The electrolyte was a 0.8 M solution of LiBOB (Chemetall) in EC:DEC (1:1 ratio by volume) purchased from Aldrich. Solvents and salt were used as received. The working electrode and the counter electrode consisting of metallic lithium were separated with a Celgard separator. The electrochemical measurements were performed on a VMP3 potentiostat/galvanostat at room temperature. For in-situ XAS study, the half-batteries with the optimal total absorption thickness (μd) of about 2 above the investigated Mn and Fe absorption edge were charged with a current density corresponding to C/30 and removed every 7.5 h for the XAS measurement, so that the nominal change in the composition was $\Delta x = 0.25$ in Li_xMSiO_4. After a XAS measurement the batteries were reconnected to the VMP3 and charged/discharged to the next level.

Reference compounds (MnO, Mn_3O_4, Mn_2O_3, MnO_2, $LiFePO_4$ and $FePO_4$) were prepared as homogeneous self-supporting pellets. Micronised powder was homogeneously mixed with micronised BN powder and pressed into pellets with the total absorption thickness of about 1.5 above the Mn or Fe K-edge.

X-ray absorption spectra of Li_2MnSiO_4 and Li_2FeSiO_4 samples and reference compounds were measured in the energy region of the Mn and Fe K-edge at room temperature in transmission detection mode at the XAFS beamline of the ELETTRA synchrotron radiation facility in Bazovica (Trieste), Italy, and at C beamline of HASYLAB at DESY, Hamburg. In both cases a Si (1 1 1) double crystal monochromator was used with about 0.8 eV resolution at XAFS beamline and 1.3 eV at C beamline at 7 keV. The intensity of the

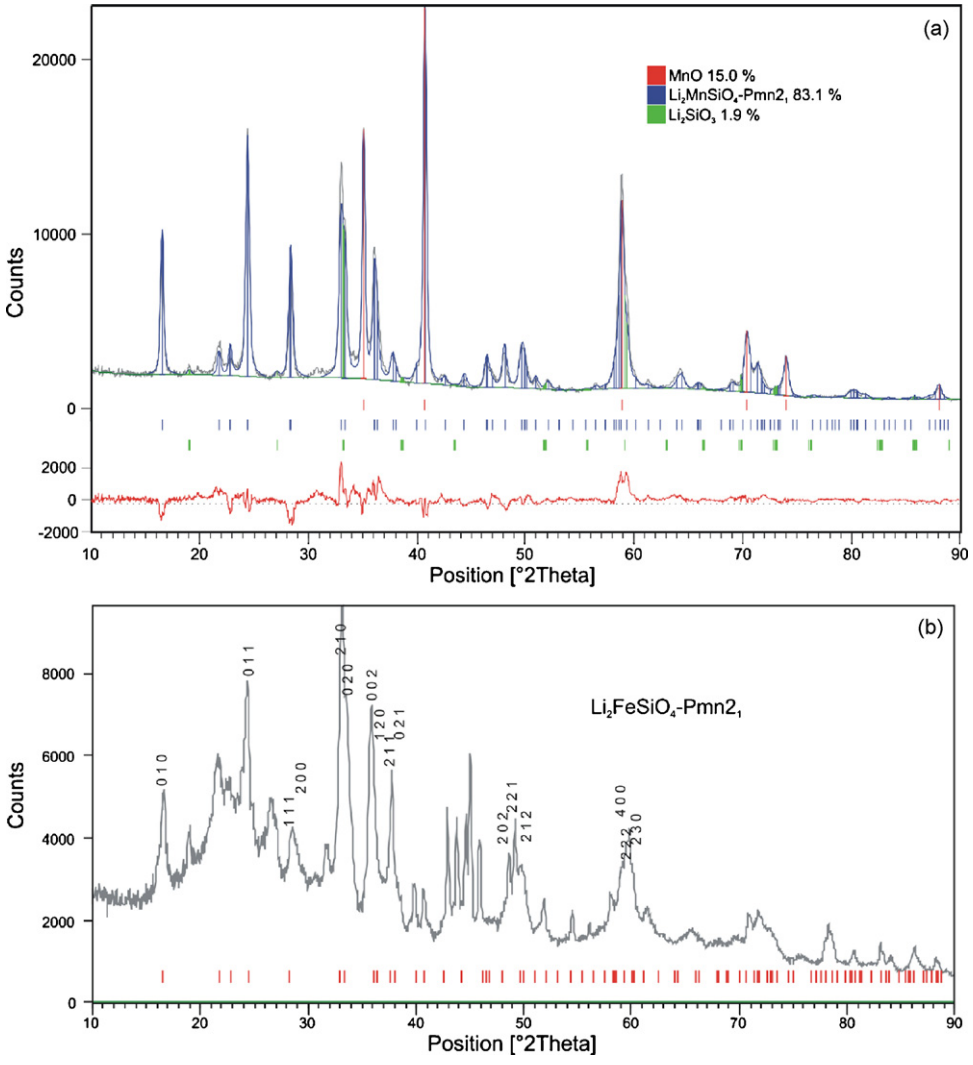

Fig. 1. X-ray diffraction patterns of (a) Li_2MnSiO_4 sample and (b) Li_2FeSiO_4 sample.

monochromatic X-ray beam was measured by three consecutive ionization detectors respectively filled with the following gas mixtures: 580 mbar N_2 and 1420 mbar He; 1000 mbar N_2, 90 mbar Ar and 910 mbar He; 1900 mbar N2 and 100 He (XAFS); 30 mbar Ar and 650 mbar N_2; 380 mbar Ar; 580 mbar Ar (C beamline). Batteries were mounted on a sample holder between the first and the second ionization detector. In the XANES region equidistant energy steps of 0.3 eV were used, while for the EXAFS region equidistant energy steps of 2 eV were adopted with an integration time of 2 s/step. In all experiments the exact energy calibration was established with simultaneous absorption measurements on 5 μm thick Mn and Fe metal foil placed between the second and the third ionization chamber. Absolute energy reproducibility of the measured spectra was ±0.05 eV.

For in-situ Mössbauer spectroscopy measurements the Li_2FeSiO_4/C sample was charged with current density of C/240 (0.7 mA g^{-1}), each measured spectrum representing an average of the composition interval $\Delta x = 0.1$ in Li_xFeSiO_4/C sample. ^{57}Fe Mössbauer experiments were performed in transmission geometry at room temperature using a constant acceleration spectrometer. The source was ^{57}Co in a Rh matrix. Velocity calibration and isomer shifts (IS) are quoted relative to an absorber of metallic iron at room temperature. Parameters were fitted with a standard least-squares fitting routine with Lorentzian lines.

X-ray powder diffraction pattern of Li_2FeSiO_4 and Li_2MnSiO_4 were collected on a Siemens D-5000 diffractometer in reflection (Bragg–Brentano) mode using Cu K_α radiation, monochromatized by a secondary graphite monochromator. The data were collected in the range between 10° and 90° in steps of 0.04° and the integration time of 8 s per step.

3. Results and discussion

3.1. XRD and Mössbauer analysis

The quality of samples prepared for in-situ X-ray absorption spectroscopy was checked with XRD and Mössbauer spectroscopy. Fig. 1a shows refined XRD pattern for Li_2MnSiO_4/C sample. Only *Pmn2₁* polymorph was used in the refinement. The obtained parameters for Li_2MnSiO_4 phase are: $a = 6.304$ (1) Å, $b = 5.377$ (9) Å and $c = 4.983$ (9) Å with the goodness of fit $R_p = 8.6$ (5)% and $R_{wp} = 10.9$ (2)%. Two additional crystalline phases were detected in the sample as impurities: MnO in the amount of about 15% and about 2% of Li_2SiO_3.

The quality of XRD pattern obtained from the Li_2FeSiO_4/C sample did not allow a good refinement (Fig. 1b). The major Bragg reflections were marked with *h k l* from *Pmn2₁* polymorph. The difficulties to fit XRD spectra from Li_2FeSiO_4/C sample most probably arose from the presence of Fe(III) (about 18 at.%) and Fe magnetic impurities (about 21 at.%) in the sample, which were detected with Mössbauer spectroscopy on the as prepared sample. We can determine the magnetic impurity in the sample as a Fe_3C phase, while the origin of non-magnetic Fe(III) is probably due to partially oxidized Li_xFeSiO_4/C sample. With the help of Mössbauer spectroscopy we were able to determine the ratio between Fe(II) and Fe(III) (0.82:0.18) in the as prepared sample. This ratio was used for calibration of the XANES spectra for Li_2FeSiO_4/C sample.

The change of oxidation state of iron in Li_2FeSiO_4/C during lithium extraction/insertion was monitored by in-situ Mössbauer analysis. Fig. 2a shows Mössbauer spectra of as prepared sample (the lowest spectrum at left column) and spectra obtained during

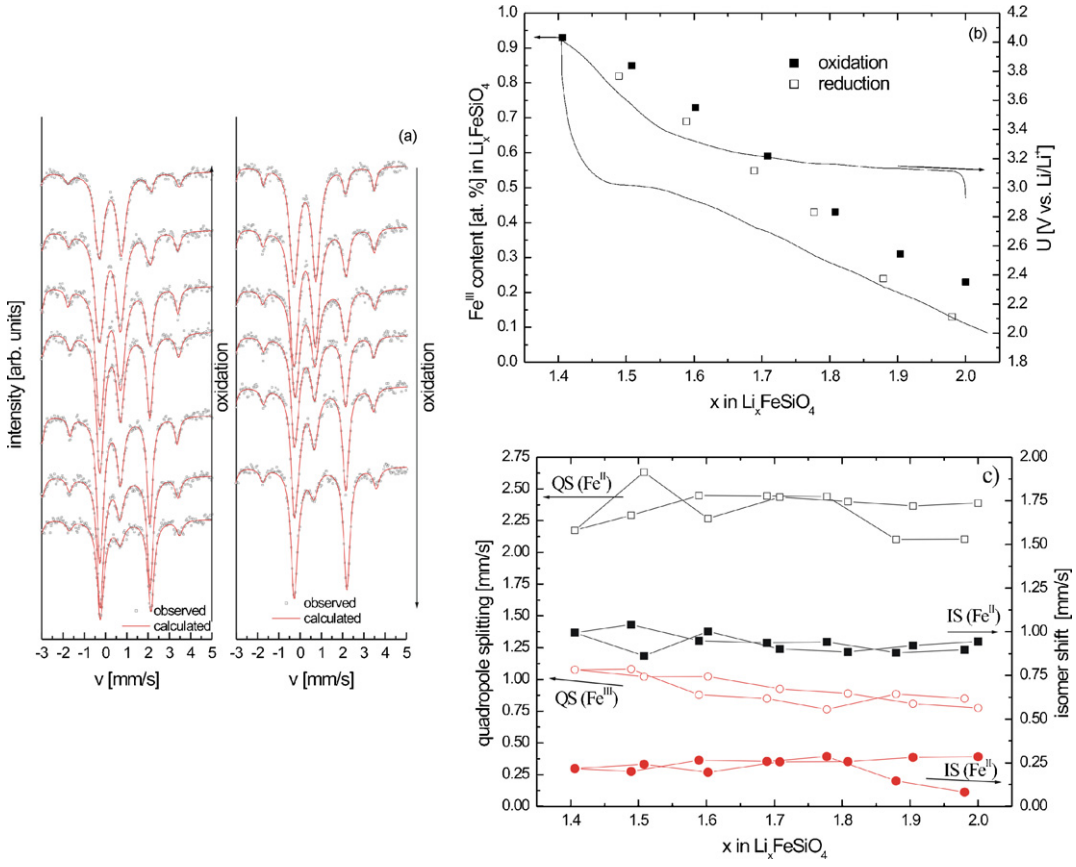

Fig. 2. (a) Set of measured and calculated Mössbauer spectra during oxidation (left column) and during reduction (right column); (b) electrochemical charge/discharge curve during in-situ Mössbauer spectroscopy (right *y*-axis) experiment and Fe(III) content (at.%) in Li_xFeSiO_4 (left *y*-axis); (c) Mössbauer parameters (QS–left axis and IS–right axis) during oxidation/reduction process.

oxidation (left column) and reduction (right column) in the first cycle. The common future of all spectra is the fact that they can be fitted with a two doublets and one sextet. Sextet, representing magnetic phase remains almost unchanged in all of spectra, while the area of doublets that correspond to Fe(II) in the tetrahedral environment and Fe(III) in the tetrahedral environment is a function of the charge passed through the battery. Area of doublets gives the content of Fe(II) and Fe(III) in the material. This one depends linearly on the charge passed through the cell (Fig. 2b right *y*-axis), providing the indirect evidence that no sporadic (irreversible) reactions are taking place in this potential range. The amount of charge passed through the battery is in the agreement with the change in the oxidation state of Fe during the oxidation/reduction process. We gained additional capacity from Fe(III) oxidized phase, which was at the beginning ascribed to $LiFeSiO_4$ (Fig. 2b, left *y*-axis). The extracted Mössbauer parameters: quadrupole splitting–QS and isomer shift–IS for Fe(II) and Fe(III), are shown in the Fig. 2c. It is worth noting that the starting Mössbauer parameters are very close to the values of Nyten [7], while in the oxidized faze ($LiFeSiO_4$) that is formed during oxidation, the QS values differ for 0.3–0.4 mm s^{-1}. The reason for observed differences in QS values is not fully understood, however we presume this difference can be ascribed to the different polymorph used in our experiment as it was used by Nyten. It is worth to mention that the existence of different polymorphs in Li_2FeSiO_4 was not proven yet, however the above opinion is based on the work on Li_2MnSiO_4 and Li_2CoSiO_4 [2,3,12,20]. Based on our in-situ Mössbauer experiment we agree with a conclusion given by Nyten [7], that local environment of iron observed with Mössbauer spectroscopy is very similar before and after "phase transition" reflected as a shift of potential from 3.1 to 2.8 V. At the end of Mössbauer part we need to emphasize that Mössbauer parameters of the magnetic phase remain very similar during the oxidation/reduction process in all fitted spectra.

3.2. XAS study

Prior to the in-situ XAS measurements the electrochemical properties of the samples were checked (dashed galvanostatic curves in Fig. 3a and b) with a current density corresponding to C/30. The XAS measurements were performed at the beginning and after every 7.5 h of charging/discharging at room temperature, at the battery oxidation/reduction states given by the points on the constructed solid galvanostatic curves, marked with letters *a*–*g*.

3.3. Mn and Fe K-edge XANES

The series of Fe K-edge and Mn K-edge XANES spectra measured during first cycle of battery charging/discharging (*a*–*g*) are shown on Figs. 4 and 5, together with reference Mn and Fe compounds with known valence states and site structure of the respective element. The presence of a weak isolated pre-edge resonance in the Fe (Fig. 4) and Mn (Fig. 5) XANES spectra of the samples is a clear evidence of the tetrahedral coordination of Fe and Mn cations in the crystal structure [21–23]. The changes in the strength of pre-edge resonance and the edge energy position and shape during first oxidation and reduction of the battery indicate the changes in the local symmetry for both cations. The shapes of the Fe XANES spectra taken on the as-prepared sample and after one or five charge/discharge cycles show no significant differences, suggesting that local symmetry of Fe cations reversibly returns to the initial one after each cycle. In the case of Li_2MnSiO_4 sample the shape of the Mn XANES spectrum after first reduction indicates that the process is not completely reversible.

The valence state of metal cation in the sample can be deduced from the energy shift of the absorption edge [21–25]. With increasing oxidation state each absorption feature in the XANES spectrum

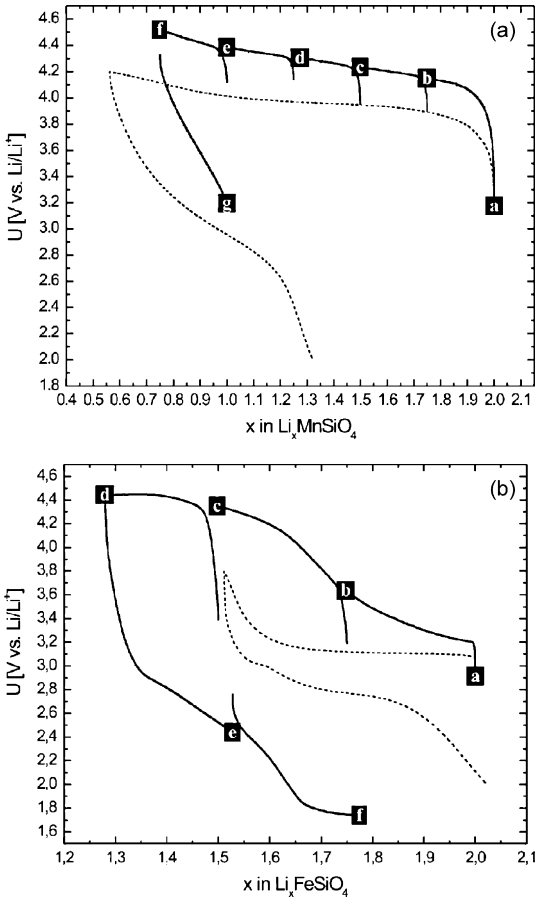

Fig. 3. Electrochemical curves (dashed lines) and constructed electrochemical curves (solid lines) for (a) Li_2MnSiO_4 sample and (b) Li_2FeSiO_4 sample. Letters on constructed curves shows the point where XAS measurements were taken.

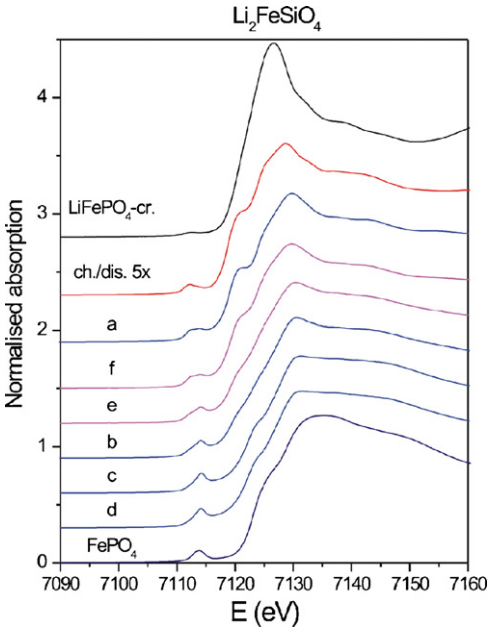

Fig. 4. The Fe K-edge XANES spectra of Li_2FeSiO_4 sample during the process of charging and discharging, and standard $LiFePO_4$ and $FePO_4$ reference compounds. The spectra are displaced vertically for clarity.

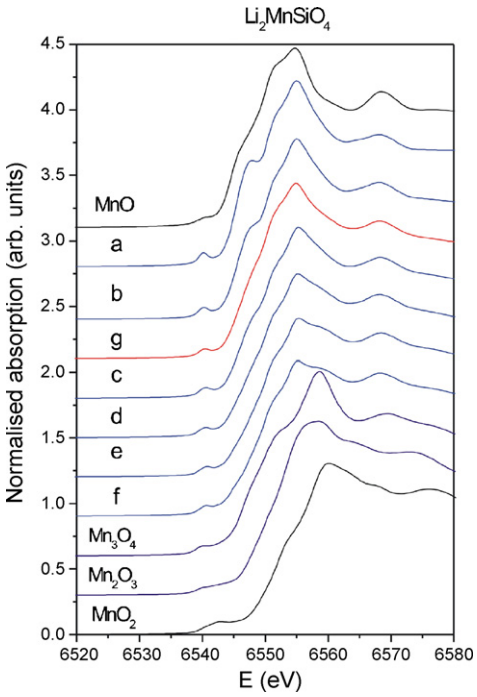

Fig. 5. The Mn K-edge XANES spectra of Li_2MnSiO_4 sample during the process of charging and discharging, and standard MnO, Mn_3O_4, Mn_2O_3, MnO_2 reference compounds. The spectra are displaced vertically for clarity.

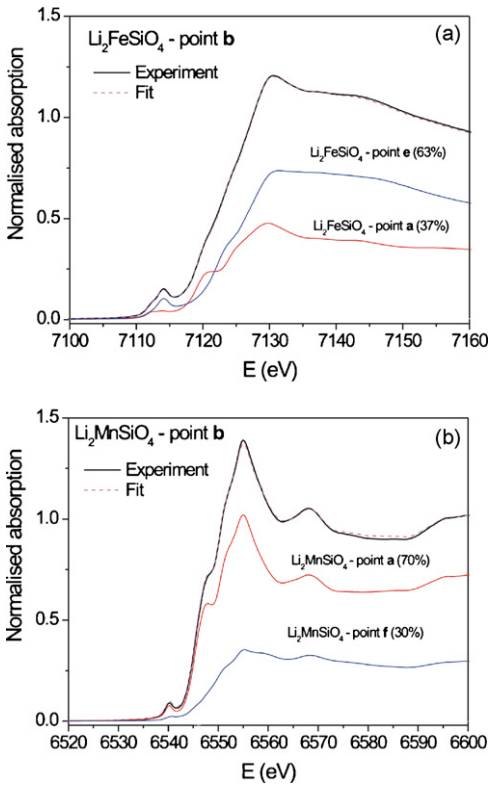

Fig. 6. (a) Fe K-edge XANES spectrum of Li_2FeSiO_4 sample in the point *b* (top); Solid line – experiment; dashed line – best-fit linear combination of XANES profiles of Li_2FeSiO_4 sample as prepared (point *a*) and after 22.5 h charging (point *d*). (b) Mn K-edge XANES spectrum of Li_2MnSiO_4 sample after 7.5 h charging (point *b*). Solid line – experiment; dashed line – best-fit linear combination of XANES profiles of Li_2MnSiO_4 sample as prepared (point *a*) and after 37.5 h charging (point *f*).

is shifted to higher energies. In Mn and Fe K-edge a shift of the edge position of about 4 eV per unit oxidation state is observed on reference compounds. If the sample contains same cation in two or more sites with different local structure and valence state, then the measured XANES spectrum is a linear combination of individual XANES spectra of different cation sites. In such cases the relative amounts of the cation at each site can be precisely determined by a linear combination fit.

This procedure is applied to Fe and Mn XANES spectra of the samples: the spectra from intermediate states can be completely described by a linear combination of the XANES spectrum of the starting (as prepared) compound, and the spectrum at the highest oxidation state (point *d* in Li_2FeSiO_4 and *f* in Li_2MnSiO_4). The quality of fit is illustrated in Fig. 6a and b. In this way we were able to determine the relative amount of each component with a precision of 1%. The relative Fe(III)/Fe(II) ratio in Li_2FeSiO_4 at the highest oxidation state (point *d*) was determined by the linear combination fit with the XANES spectrum of the starting Li_2FeSiO_4 compound and the XANES spectrum of $FePO_4$ as a reference for tetrahedrally coordinated Fe(III) cations. In case of Li_2FeSiO_4/C the composition of the as prepared sample (point *a*) was determined with Mössbauer spectroscopy. The sample contains 61 at.% of tetrahedral Fe(II) and 18 at.% tetrahedral Fe(III) in the crystal structure of Li_2FeSiO_4. The remaining 21 at.% is magnetic iron in the form of Fe_3C. This impurity phase, as it was observed also with Mössbauer spectroscopy, does not change during battery operation.

In the case of Li_2MnSiO_4 the composition of as prepared sample (point *a*) was determined by XRD analysis, which showed about 15 wt.% of impurity in the form of crystalline MnO. All Mn in the as prepared sample was thus in divalent form. The result is confirmed by the comparison of the Mn K-edge energy position of the as prepared sample with reference spectrum of MnO. The Mn(III)/Mn(II) relative ratio in Li_2MnSiO_4 at the highest oxidation state (point *f*) was determined by the linear combination fit with the reference XANES spectrum of MnO as a reference for Mn(II) and the XANES spectrum of Mn_2O_3 as a reference for Mn(III). The transition from Mn(II) to Mn(III) occurs in the potential range from 4.0 to 4.5 V vs. metallic lithium.

The results on the change of relative ratio of Mn(III)/Mn(II) and Fe(III)/Fe(II) in the intermediate states of the samples during Li_2MnSiO_4/C and Li_2FeSiO_4/C material oxidation and reduction are summarized in the Fig. 7. During Li_2FeSiO_4 battery charging the relative amount of Fe(III) gradually increased from 18% to 73%, while in charging of Li_2MnSiO_4 60% of Mn(II) is oxidized to Mn(III) indicating that less than 1 mol of Li is removed from the crystal structure in each case. After discharging both relative ratios of Mn(III)/Mn(II)

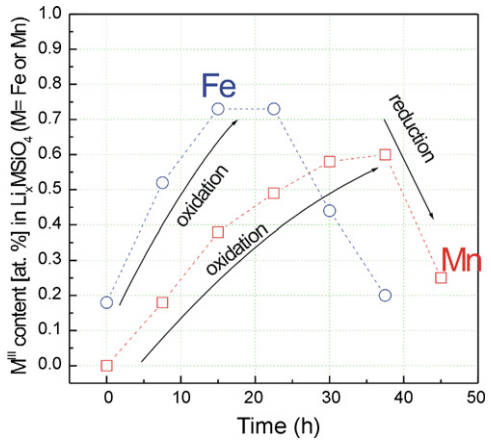

Fig. 7. Change of Fe and Mn valence during battery charging and discharging in the Li_2FeSiO_4 and Li_2MnSiO_4 samples.

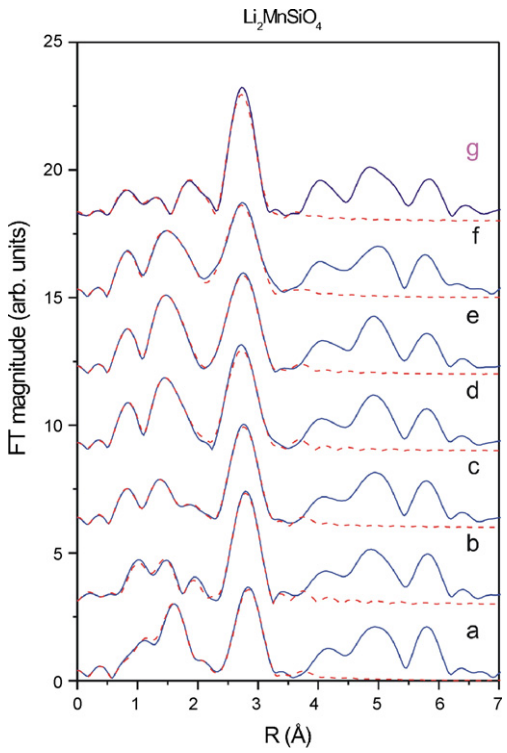

Fig. 8. Fourier transform of k^3-weighted Mn EXAFS spectra of Li_2MnSiO_4 samples, calculated in the k range of 3.0–12 $Å^{-1}$. Experiment – (solid line); EXAFS model–(dashed line).

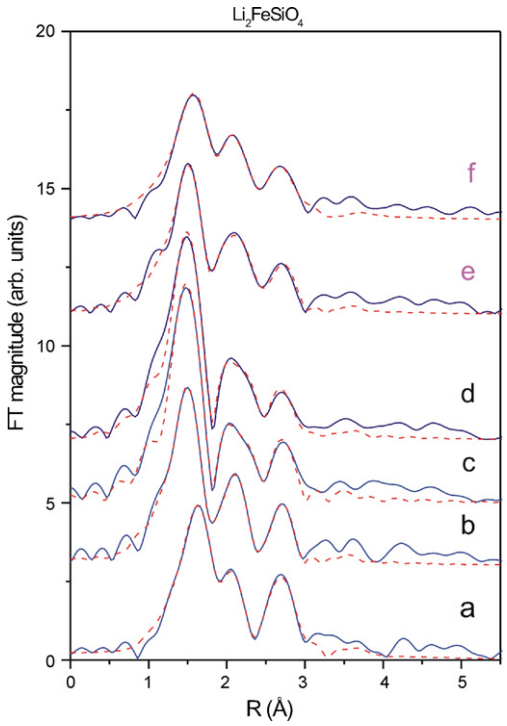

Fig. 9. Fourier transform of k^3-weighted Fe EXAFS spectra of Li_2FeSiO_4 sample during the process of charging and discharging, calculated in the k range of 3.0–14 $Å^{-1}$. Experiment – (solid line); EXAFS model – (dashed line).

and Fe(III)/Fe(II) return to the initial state of the as prepared sample.

3.4. Mn and Fe K-edge EXAFS analysis

The short-range order around Mn and Fe cations in Li_2FeSiO_4/C and Li_2MnSiO_4/C cathode materials during oxidation and reduction is directly probed by Mn K-edge and Fe K-edge EXAFS analysis [26,27]. Contributions of several consecutive shells of neighbours are visible up to about 7 Å in Mn spectra (Fig. 8), and up to about 3.5 Å in Fe spectra (Fig. 9). Both cations show well ordered yet significantly different local surroundings. The series of the FT spectra reveal significant changes in the local structure around Mn and Fe cations during one cycle of battery charging and discharging. The changes, however, are limited to the nearest coordination shells, while the structure of coordination shells beyond $R > 2.7$ Å remains practically unchanged.

The quantitative analysis of Fe and Mn K-edge EXAFS spectra is performed with the IFEFFIT program package [27]. Structural parameters are quantitatively resolved by comparing the measured signal with model signal, constructed with the FEFF6 program code [28] in which the photoelectron scattering paths are calculated *ab initio* from a tentative spatial distribution of neighbour atoms, based on the unit cell parameters of the orthorhombic Li_2MnSiO_4 crystal structure with *Pmn21* space group. In this structure Mn cations are tetrahedrally coordinated to four oxygen atoms (two at 2.03 Å and two at 2.10 Å). In more distant coordination shells there is one oxygen atom at 2.89 Å, followed by alternate Si and Li neighbours (one Si at 2.98 Å, four Li at 3.07 Å, two Li at 3.11 Å, two Si at 3.16 Å, two Li at 3.18 Å, and one Si at 3.21 Å). The same model of local environment of Fe cations is used for Li_2FeSiO_4. The EXAFS model comprises all single scattering paths up to 3.30 Å. The one multiple-scattering path within this range is omitted as insignificant.

A very good agreement between the model and the experimental spectra is found in the R range from 1.3 to 3.6 Å for Mn (Fig. 8) and from 1.3 to 3.2 Å. for Fe spectra (Fig. 9). The number of variable parameters in the model was minimised to reduce correlations. Variations of the neighbour positions in each neighbour shell ΔR_i, the neighbour coordination numbers N_i at each position, a separate Debye-Waller factor (σ_1^2) for each type of neighbouring atoms and a common shift of energy origin ΔE_0 were included. Since the contribution of Li atoms in EXAFS signal was very weak, the coordination numbers and Debye-Waller factors for the Li shells could not be reliably determined in the fitting procedure; rather, they were kept fixed. The Li coordination number was adequately adjusted for each spectrum according to the battery oxidation/reduction state. Similarly, the EXAFS amplitude reduction factor $S_0{}^2$ for Fe and Mn was kept fixed at the respective values of 0.75 and 0.72. Best fit parameters of nearest coordination shells, undergoing the main structural changes are collected in Tables 1 and 2. In more distant coordination shells (2.8 Å < R_i < 3.3 Å) only minor variation in neighbor distances (ΔR_i < 0.1 Å) is detected, presumably due to the relaxation of the crystal structure, so the structural parameters are not listed.

In the interpretation of the structural parameters of the nearest Fe coordination shells we took into account that the Li_2FeSiO_4 samples contained also about 21 at.% of Fe impurities in the form of Fe_3C nanoparticles, as suggested by Mössbauer spectroscopy analysis. The contribution of the metallic Fe impurities is modelled by a shell of two Fe neighbours at 2.54 Å (in agreement with local Fe neighbourhood in Fe_3C with Pbnm crystal structure, where Fe is coordinated with 12 Fe atoms at that distance).

EXAFS results for the local Mn environment in the as synthesized Li_2MnSiO_4 (point *a*) are in agreement with XRD data. Mn is located in a distorted tetrahedron with two oxygen atoms at 2.04 Å and two oxygen atoms at 2.19 Å. During the oxidation the short Mn–O bond decreases from 2.04 to 1.87 Å in a correlation with the increase of Mn valence state, while the larger Mn–O distance remains unchanged. The reduction is not completely reversible. The

Table 1
Parameters of the nearest coordination shells around Mn atoms in Li_2MnSiO_4 samples at different stages of charge/discharge process: the number of nearest neighbour atoms (oxygen) (N_O), distance (R), and Debye-Waller factors (σ^2). Best fit in the k range from 3.5 to 12 Å^{-1} and the R range from 1.3 to 3.6 Å is obtained with amplitude reduction factor $S_0^2 = 0.72$. Uncertainty of the last digit is given in parentheses.

No	R [Å]	σ^2 [Å^2]
Li_2MnSiO_4 – *a*		
2.4 (4)	2.04 (1)	0.006 (2)
1.6 (4)	2.19 (1)	0.006 (2)
b		
2.1 (4)	1.96 (1)	0.009 (2)
1.9 (4)	2.16 (1)	0.009 (2)
c		
2.2 (4)	1.92 (1)	0.007 (2)
1.8 (4)	2.18 (1)	0.007 (2)
d		
2.3 (4)	1.89 (1)	0.006 (2)
1.7 (4)	2.18 (1)	0.006 (2)
e		
2.2 (4)	1.87 (2)	0.006 (2)
1.8 (4)	2.21 (2)	0.006 (2)
f		
2.1 (4)	1.87 (2)	0.007 (2)
1.9 (4)	2.23 (2)	0.007 (2)
g		
1.6 (4)	1.91 (1)	0.007 (2)
2.4 (4)	2.16 (1)	0.007 (2)

distribution of oxygen atoms at the two distances in the MnO_4 tetrahedron after the reduction (point *g*) differs from that in the point *a*.

Fe EXAFS results show that Fe cations in the as synthesized Li_2FeSiO_4 (point *a*) are coordinated by four oxygen atoms – three at 1.98 Å and one at 2.40 Å. The result indicates that Fe cations are located off the center of the FeO_4 tetrahedron in the crystal structure, shifted towards the three oxygens in the tetrahedral plane and consequently further from the apical oxygen. During the oxidation both Fe–O distances decrease with the increase of the relative amount of Fe(III). After the reduction (point *f*) the local environment of Fe is the same as in the as prepared sample (point *a*).

Table 2
Parameters of the nearest coordination shells around Fe atoms in Li_2FeSiO_4 samples at different stages of charge/discharge process: the number of nearest neighbour atoms (oxygen) (No), distance (R), and Debye-Waller factors (σ^2). Best fit in the k range from 3 to 14 Å^{-1} and the R range from 1.3 to 3 Å is obtained with amplitude reduction factor $S_0^2 = 0.75$. Uncertainty of the last digit is given in parentheses.

No	R [Å]	σ^2 [Å^2]
Li_2FeSiO_4 – *a*		
3.4 (4)	1.98 (1)	0.007 (2)
1.4 (5)	2.40 (1)	0.007 (2)
b		
3.3 (4)	1.88 (1)	0.006 (2)
1.4 (5)	2.29 (1)	0.006 (2)
c		
3.3 (4)	1.85 (1)	0.004 (2)
1.4 (5)	2.28 (1)	0.004 (2)
d		
3.3 (4)	1.86 (1)	0.004 (2)
1.4 (5)	2.27 (1)	0.004 (2)
e		
3.2 (4)	1.89 (1)	0.006 (2)
1.0 (5)	2.29 (1)	0.006 (2)
f		
3.1 (4)	1.97 (1)	0.007 (2)
1.4 (5)	2.44 (1)	0.007 (2)

To summarize XAS part we can conclude that both analyzed materials return in its original oxidation state after the oxidation/reduction cycle and in neither case we were not able to detect oxidation state higher than 3+. At this point we are not able to give a clear answer if this limitation (not obtaining oxidation state 4+) is due to kinetics or thermodynamic properties of Li_2MSiO_4 (M = Fe or Mn) materials. From the point of structural reversibility the oxidation/reduction process is reversible for Fe analogue, with a slight relaxation in the local environment, while the distortion of oxygen atoms in MnO_4 tetrahedron after the reduction is different from the one at the beginning, nevertheless the oxidation state of manganese is 2+. Irreversible changes in the local environment of Mn and the fact that we did not detect the change of oxidation state from Mn(II) to Mn(IV) are strong indictors that Li_2MnSiO_4 by itself is probably not suitable as a cathode material, however those observations do not prejudice the use of $Li_2(Fe,Mn)SiO_4$ solid solutions as it was proposed [4].

4. Conclusion

We showed that the changes in the Fe and Mn local environment of two iso-structural materials, Li_2FeSiO_4 and Li_2MnSiO_4 during the oxidation/reduction process in the first cycle do not run in parallel. The changes in the local environment of iron in Li_2FeSiO_4/C material are reversible. Mössbauer parameters return unchanged after first cycle and the change in the oxidation state of iron at any point of the cycle is in agreement with the charge passed through the cell. The same conclusion follows from XANES spectra. Structural parameters from EXAFS shows that the local environment of Fe changes only within the immediate oxygen envelope up to 2.6 Å during oxidation, and that it is preserved after the subsequent reduction with a slight relaxation in the structure. Complete reversible changes in the local environment are good preliminary conditions for stable, long term life of Li_2FeSiO_4. The XAS results on Li_2MnSiO_4/C material show that the changes in the oxidation state of Mn are limited to the Mn(II) – Mn(III) range and that the related changes in the local environment of Mn are not reversible. The irreversible changes could be correlated to the loss of crystallinity during oxidation as recently shown in an in-situ XRD experiment.

Acknowledgements

This research was supported by the Slovenian Research Agency, by Ministry of Education, Science and Sport of Slovenia (MNT ERA-net project) and the support from the European Network of Excellence 'ALISTORE' network is acknowledged. The financial support, by DESY, ELETTRA and the European Community under the FP6 Programme "Structuring the European Research Area" contract RII3-CT-2004-506008 (IA-SFS). Access to synchrotron radiation facilities of ELETTRA (beamline XAFS) and HASYLAB at DESY (beamline C) is acknowledged. We would like to thank Luca Olivi from XAFS beamline of ELETTRA and Edmund Welter of HASYLAB for expert advice on beamline operation.

References

[1] A. Nyten, A. Aboumrane, M. Armand, T. Gustafson, J.O. Thomas, Electrochem. Commun. 7 (2005) 156–160.
[2] R. Dominko, M. Bele, M. Gaberscek, A. Meden, M. Remskar, J. Jamnik, Electrochem. Commun. 8 (2006) 217–222.
[3] C. Lyness, B. Delobel, A.R. Armstrong, P.G. Bruce, Chem. Commun. 46 (2007) 4890–4892.
[4] Z.L. Gong, Y.X. Li, Y. Yang, Electrochem. Solid-State Lett. 9 (2006) A542–A544.
[5] K. Zaghib, A. Ait Salah, N. Ravet, A. Mauger, F. Gendron, C.M. Julien, J. Power Sources 160 (2006) 1381–1386.
[6] A.K. Padhi, K.S. Nanjundaswamy, J.B. Goodenough, J. Electrochem. Soc. 144 (1997) 1188–1194.
[7] A. Nyten, S. Kamali, L. Haggstrom, T. Gustafsson, J.O. Thomas, J. Mater. Chem. 16 (2006) 2266–2272.

[8] A. Nyten, M. Stjerndahl, H. Rensmo, H. Siegbahn, M. Armand, T. Gustafsson, K. Edstrom, J.O. Thomas, J. Mater. Chem. 16 (2006) 3483–3488.
[9] A. Kokalj, R. Dominko, M. Gaberscek, M. Bele, G. Mali, M. Remskar, J. Jamnik, Chem. Mater. 19 (2007) 3633–3640.
[10] R. Dominko, M. Bele, A. Kokalj, M. Gaberscek, J. Jamnik, J. Power Sources 174 (2007) 457–461.
[11] R. Dominko, D.E. Conte, D. Hanzel, M. Gaberscek, J. Jamnik, J. Power Sources 178 (2007) 842–847.
[12] M.E. Arroyo y de Dompablo, R. Dominko, J.M. Gallardo-Amores, L. Dupont, G. Mali, H. Ehrenberg, J. Jamnik, E. Moran, Chem. Mater. 20 (2008) 5574–5584.
[13] R. Dominko, J. Power Sources 184 (2008) 462–468.
[14] A.J. Jacobson, L.E. McCandlish, J. Solid State Chem. 29 (1979) 355–365.
[15] A.S. Anderson, B. Kalska, L. Haggstrom, J.O. Thomas, Solid State Ionics 130 (2000) 41–52.
[16] M.E. Arroyo-de Dompablo, M. Armand, J.-M. Tarascon, U. Amador, Electrochem Commun. 8 (2006) 1292–1298.
[17] A. Deb, U. Bergmann, S.P. Cramer, E.J. Cairns, Electrochim. Acta 50 (2005) 5200–5207.
[18] K.-W. Nam, M.G. Kim, K.-N. Kim, J. Phys. Chem. C 111 (2007) 749–758.
[19] M.P. Pechini, US. Patent no 3,330,697, July 1967.
[20] V.V. Politaev, A.A. Petrenko, V.B. Nalbandyan, B.S. Medvedev, E.S. Shvetsova, J. Solid. State Chem. 180 (2007) 1045.
[21] J. Wong, F.W. Lytle, R.P. Messmer, D.H. Maylotte, Phys. Rev. B 30 (1984) 5596–5610.
[22] A. Bianconi, J. Garcia, M. Benfatto, A. Marcelli, C.R. Natoli, M.F. Ruiz-Lopez, Phys. Rev. B 43 (1991) 6885–6892.
[23] I. Arčon, J. Kolar, A. Kodre, D. Hanžel, M. Strlič, X-ray Spectrom. 36 (2007) 199–205.
[24] N. Zabukovec Logar, N. Novak Tušar, G. Mali, M. Mazaj, I. Arčon, D. Arčon, A. Rečnik, A. Ristić, V. Kaučič, Microporous Mesoporous Mater. 96 (2006) 386–395.
[25] R. Dominko, M. Bele, J.M. Goupil, M. Gaberscek, D. Hanzel, I. Arcon, J. Jamnik, Chem. Mater. 19 (2007) 2960–2969.
[26] D.C. Koningsberger, R. Prins, X-ray Absorption, Principles, Techniques of EXAFS, SEXAFS and XANES, John Wiley & Sons, New York, 1988, ISBN 0-471-87547-3.
[27] B. Ravel, M. Newville, J. Synchrotron Radiat. 12 (2005) 537.
[28] J.J. Rehr, R.C. Albers, S.I. Zabinsky, Phys. Rev. Lett. 69 (1992) 3397–3400.